AIP | Review of Scientific Instruments

High resolution polarimeter-interferometer system for fast equilibrium dynamics and MHD instability studies on Joint-TEXT tokamak (invited)a)

J. Chen, G. Zhuang, Q. Li, Y. Liu, L. Gao, Y. N. Zhou, X. Jian, C. Y. Xiong, Z. J. Wang, D. L. Brower, and W. X. Ding

Citation: Review of Scientific Instruments **85**, 11D303 (2014); doi: 10.1063/1.4891603
View online: http://dx.doi.org/10.1063/1.4891603
View Table of Contents: http://scitation.aip.org/content/aip/journal/rsi/85/11?ver=pdfcov
Published by the AIP Publishing

High resolution polarimeter-interferometer system for fast equilibrium dynamics and MHD instability studies on Joint-TEXT tokamak (invited)[a)]

J. Chen,[1] G. Zhuang,[1,b)] Q. Li,[1] Y. Liu,[1] L. Gao,[1] Y. N. Zhou,[1] X. Jian,[1] C. Y. Xiong,[1] Z. J. Wang,[1] D. L. Brower,[2] and W. X. Ding[2]

[1]*State Key Laboratory of Advanced Electromagnetic Engineering and Technology, Huazhong University of Science and Technology, Wuhan 430074, China*

[2]*Department of Physics and Astronomy, University of California Los Angeles, Los Angeles, California 90095, USA*

(Presented 2 June 2014; received 29 May 2014; accepted 17 July 2014; published online 5 August 2014)

A high-performance Faraday-effect polarimeter-interferometer system has been developed for the J-TEXT tokamak. This system has time response up to 1 μs, phase resolution $< 0.1^\circ$ and minimum spatial resolution $\sim$15 mm. High resolution permits investigation of fast equilibrium dynamics as well as magnetic and density perturbations associated with intrinsic Magneto-Hydro-Dynamic (MHD) instabilities and external coil-induced Resonant Magnetic Perturbations (RMP). The 3-wave technique, in which the line-integrated Faraday angle and electron density are measured simultaneously by three laser beams with specific polarizations and frequency offsets, is used. In order to achieve optimum resolution, three frequency-stabilized HCOOH lasers (694 GHz, >35 mW per cavity) and sensitive Planar Schottky Diode mixers are used, providing stable intermediate-frequency signals (0.5–3 MHz) with S/N > 50. The collinear R- and L-wave probe beams, which propagate through the plasma poloidal cross section (a = 0.25–0.27 m) vertically, are expanded using parabolic mirrors to cover the entire plasma column. Sources of systematic errors, e.g., stemming from mechanical vibration, beam non-collinearity, and beam polarization distortion are individually examined and minimized to ensure measurement accuracy. Simultaneous density and Faraday measurements have been successfully achieved for 14 chords. Based on measurements, temporal evolution of safety factor profile, current density profile, and electron density profile are resolved. Core magnetic and density perturbations associated with MHD tearing instabilities are clearly detected. Effects of non-axisymmetric 3D RMP in ohmically heated plasmas are directly observed by polarimetry for the first time. [http://dx.doi.org/10.1063/1.4891603]

I. INTRODUCTION

Tokamak plasma is confined by magnetic field generated by external magnetic coils and self-carrying plasma current. The profile of magnetic field, or equivalently the safety factor profile, is closely related to the equilibrium and stability of the plasma and has critical importance in tokamak physics research as well as advanced operation. Consequently the measurement of core magnetic field and its temporal dynamics is considered as one of those indispensable diagnostics for modern tokamak study.[1] In addition, as the development of diagnostic technology advances, measurement of core plasma magnetic field perturbations related to intrinsic instabilities and externally imposed non-axisymmetric effects have become an important area of plasma control and physics studies.

After several decades of exploration, laser-based Faraday-effect polarimetry is now a promising candidate for measurement of equilibrium magnetic field and its perturbation in the core plasma. The principle of polarimetry as a plasma diagnostic was first proposed in 1972.[2] The intrinsic similarity between polarimetry and interferometry makes them possible to be combined for multi-field measurement. Since 1970, several different techniques have been proposed for polarimetric measurement and one of those techniques, the three-wave technique, a variation of which was first proposed by Dodel and Kunz in 1976,[3] has been largely developed in recent years. This technique has intrinsic high time response and phase resolution. The applications of this technique on MST and Alcator C-Mod have successfully lead to observation of magnetic field perturbation during Magneto-Hydro-Dynamic (MHD) activity and even high frequency fluctuation, along with electron density perturbation and fluctuation if the third wave is utilized.[4,5]

To explore the equilibrium and perturbation of magnetic field and electron density, especially the fine structure of perturbation during MHD activity, a high resolution polarimeter-interferometer system (POLARIS) based on three-wave technique has been developed on J-TEXT tokamak.[6–8] To achieve this goal, J-TEXT POLARIS is intentionally developed with high phase resolution (less than 0.1° for Faraday angle and less than 1° for line-integrated density at 50 kHz bandwidth), high temporal resolution (<1 μs), high spatial resolution (15 mm minimum) and high spatial coverage (multiple chords covering the entire plasma cross section). In this paper the diagnostic and its application will be presented. The paper

[a)]Invited paper, published as part of the Proceedings of the 20th Topical Conference on High-Temperature Plasma Diagnostics, Atlanta, Georgia, USA, June 2014.

[b)]Author to whom correspondence should be addressed. Electronic mail: ge-zhuang@hust.edu.cn

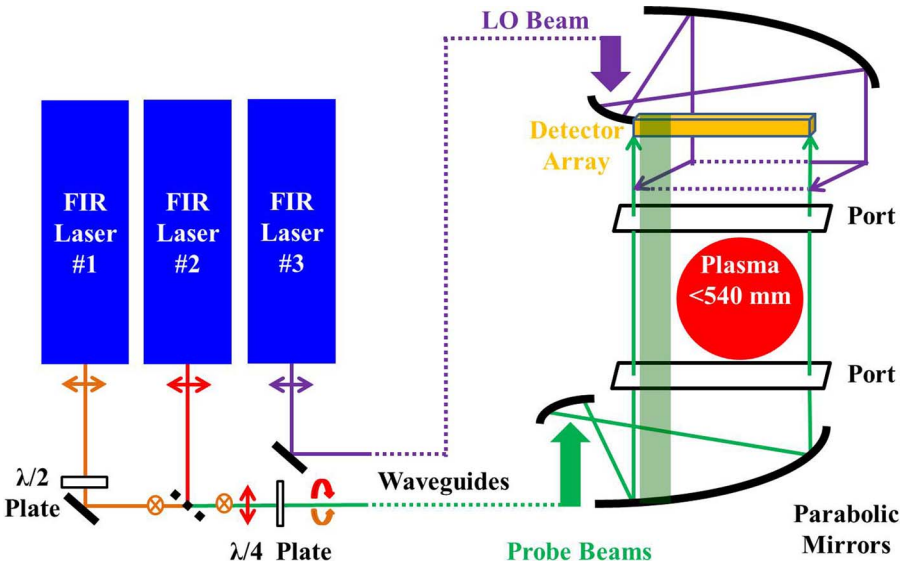

FIG. 1. Layout of J-TEXT POLARIS diagnostic (not to scale).

is organized as follows: in Sec. II the J-TEXT POLARIS is introduced in detail, including principle of measurement, optical layout, key components, protection, and calibration. Section III presents typical experimental observations and applications using POLARIS diagnostic, including equilibrium reconstruction, sawtooth oscillation, tearing mode, and Resonant Magnetic Perturbation (RMP) study. Summary is given in Sec. IV.

II. J-TEXT POLARIS

A. Principle

The three-wave technique uses three laser beams with slightly shifted frequencies and specific polarizations for simultaneous polarimetric and interferometric measurement. Two laser beams, L-beam and R-beam with counter-rotating circular-polarization, are collinearly aligned and launched into the plasma, while the third laser beam with linear polarization serves as Local-oscillator (LO). For purpose of heterodyne measurement, frequencies of the three beams are slightly offset with no overlap between the three intermediate frequencies (IF) that are produced (typically 1, 1.5, and 2.5 MHz). Each IF carries different plasma information multiplexed into a single time series for each chord, which can be isolated by band-pass filtering. Then the phase change at each IF can be calculated by phase comparison with the signal from a reference mixer.[9] The laser frequency (694 GHz) is far larger than plasma frequency (~90 GHz) and electron cyclotron frequency (~56 GHz). Phase difference between L beam or R beam with LO beam are φ_L and φ_R, respectively, while the Faraday effect is derived from the phase difference between the L beam and R beams. The Faraday angle α and line-integrated density φ are obtained from the following relations: $\alpha=(\varphi_R - \varphi_L)/2$, $\varphi = (\varphi_R + \varphi_L)/2$. It should be noted that the bandwidth of the filter used plays an important role here: normally narrower bandwidth leads to higher signal/noise ratio and consequently higher phase resolution of the measurement. Wider bandwidth leads to higher temporal resolution with the maximum available bandwidth (highest time response) limited by the IF separation. Experimentally, we have simultaneously achieved phase resolution of $<0.1^\circ$ and temporal resolution of <10 μs.[4] Therefore, the three-wave technique is capable of both high resolution and fast time response polarimetric and interferometric measurements.

B. Layout

The optical layout of the J-TEXT POLARIS diagnostic, which employs three FIR lasers, is shown in Figure 1. The initial polarization of each laser beam is linear. To perform a three-wave measurement, the polarization of laser beam #1 is rotated 90° by a half-wave plate and collinearly combined with laser beam #2. The combined beams are then transformed into circularly polarized counter-rotating R-beam and L-beam using a quarter wave plate. The combined probe beams and the linearly polarized LO beam are transported from the laser room to the tokamak hall (~11 m) by overmode circular dielectric waveguide (100 mm diameter). To optimize spatial coverage and take full advantage of large top-bottom vertical ports (610 mm × 70 mm) on J-TEXT, the probe beams and LO beams are expanded in one dimension by ×10 using two pairs of parabolic mirrors. The fully expanded size is 600 mm (along the major radius) × 60 mm (along the toroidal direction). The expanded probe beams propagate through the plasma column, combine with the LO beam and are then focused onto the linear detector array. After detection, the signal is amplified and digitized using 16 bit 10 Ms/s digitizer to preserve the raw time series data for each chord. With the expanded probe beams, the entire plasma cross section (a = 0.25–0.27 m) is fully covered. Multi-chord measurement is easily achieved by arranging the detectors in a linear array, with the spatial resolution limited by detector width. In addition, the part of the probe beams, which does not pass through the plasma column (green shadow region in Fig. 1),

is used as reference and serves to cancel phase contamination from mechanical vibration.

As the phase resolution of the measurement largely relies on the Signal/Noise Ratio (SNR) in each mixer, use of high laser power and sensitive, low-noise detector is very important. For J-TEXT POLARIS, three SIFIR-50 Coherent Inc. made Far-infrared (FIR) lasers are used. Each FIR cavity is pumped by an independent CO_2 laser ($\sim$50 W), providing a maximum FIR power output $>$35 mW/cavity. The laser wavelength used is 432 μm, and corresponding maximum Faraday angle for typical J-TEXT plasmas is $\sim5^\circ$. The FIR cavity length can be adjusted accurately for selection of intermediate frequency (i.e., laser frequency offset). Each CO_2 laser is frequency-locked using a Fabry-Perot cavity for stability. The detector array is composed of planar-diode Schottky mixers made by Virginia Diode Inc., with sensitivity $\sim$750 V/W and optimized for 694 GHz. The width of each mixer is 15 mm; thereby limiting the minimum chord spacing to 15 mm and allowing up to 36 chords across the 600 mm expanded beam. Currently 14 chords with chord spacing 30–35 mm are employed. The frequency response of the mixer- amplifier system is larger than 3 MHz, so that the highest temporal resolution is less than 1 μs.

With low phase noise and high temporal resolution, the measurement is susceptible to contamination from environmental noise. In order to shield against these deleterious effects, the laser system is placed a remote room, which is outside the biological shield and $\sim$11 meters away from J-TEXT machine to avoid possible influence of magnetic field. The laser room is temperature-controlled within 1 °C, electro-magnetically and acoustically shielded with restricted access to maintain a clean room and safety. To resist the mechanical vibration caused by the machine, the primary optical supporting structures, e.g., laser table and *in situ* optical tower for detectors and beam expanding optics, are designed and built with large mass and rubber absorbers for mechanical vibration damping. Additionally, there are also many protection elements along the optical path of J-TEXT POLARIS, e.g., electro-magnetic shielding, optical absorber and acoustic shielding to reduce corresponding interference.

With high laser power, sensitive detectors, and low background noise, we achieve high SNR and consequently low phase noise measurement is assured. For J-TEXT POLARIS, SNR is normally $>$50 for all chords. With no plasma, Root-Mean-Square (RMS) noise for Faraday angle measurement is less than 0.05° and for line-integrated density measurement is less than 1° at 50 kHz bandwidth.

C. Systematic errors

Measurement accuracy is directly determined by the identification and minimization of systematic errors. For interferometric measurement, mechanical vibration is a major error source, which can easily induce error up to tens of degrees. For J-TEXT POLARIS, the part of probe beam that does not pass through the plasma, but does pass through the vacuum vessel, provides an excellent reference which serves to cancel vibration-induced error. With this *in situ* reference, the phase error caused by vibration for interferometric measurement is less than 1°. For polarimetric measurement, systematic errors come from non-collinear (spatially offset) probe beams, polarization distortion by optical components, instability of intermediate frequency, misalignment to the toroidal field, finite-temperature effects, and Cotton-Mouton effect. Collinearity and polarization errors are major sources of systematic errors for J-TEXT POLARIS and will be discussed later. Error due to unstable intermediate frequency is associated with the path difference between probe beams and reference beam.[10] The probe beams of J-TEXT POLARIS are aligned perpendicular to the direction of toroidal field ($90^\circ \pm 0.1^\circ$), in which case error due to the misalignment to toroidal field is less than noise level. For the J-TEXT optical arrangement, the path of probe beams is equal to reference beam, therefore this error is automatically eliminated. The plasma temperature of J-TEXT experiment is normally less than 1 keV so that finite-temperature effects are ignorable.[11] The Cotton-Mutton effect and Faraday Effect for J-TEXT case is small enough, therefore the interaction between Faraday effect and Cotton-Mutton effect is weak and corresponding error is negligible (of same order or less than noise level).[12]

Faraday-effect measurement requires collinear counter-rotating circular polarization probe beams. For J-TEXT, this is achieved by using a polarization sensitive beam splitter to combine two orthogonal linearly polarized beams and quarter-wave plate to transform the combined beams to counter-rotating circular polarization. Probe beam polarization is sensitive to the accuracy and alignment of the quarter wave plate, as well as other optical components, e.g., wire-mesh beam-splitters or crystal quartz windows which have anisotropic reflection/transmission properties that may distort the polarization. For J-TEXT POLARIS, benefitting from the beam expanding optics, there are just a few optical components in the path of probe beams and no anisotropic components are used. Therefore, polarization calibration is mainly determined by the quarter wave plate alignment. A practical method to examine the polarization of counter-rotating circularly polarized probe beams is polarization modulation.[13] To accomplish this, we add a rotating (few Hz) half-wave plate in the optical path to replace the plasma and modulate the polarization. If the probe beams' polarizations are counter-rotating circularly polarized, phase difference between the R beam and L beam will change linearly and equal four times the rotation angle of the half wave plate; any distortion of polarization will lead to a nonlinear response. The result of calibration for J-TEXT POLARIS using this method is shown in Figure 2(a). A linear calibration curve is observed indicating no distortion of the probe beam polarization throughout the optical system.

A second important source of systematic error stems from non-collinearity of the probe beams and is a unique issue to three-wave measurement. When the L beam and R beam are not colinear, phase error will be introduced by the difference of their optical path length and the different plasma regions probed. This error source becomes more important if there is a steep electron density gradient. Even a millimeter misalignment or small angular displacement can introduce phase error of same order as the Faraday angle.[14] Fortunately, the colinearity error can be directly examined in

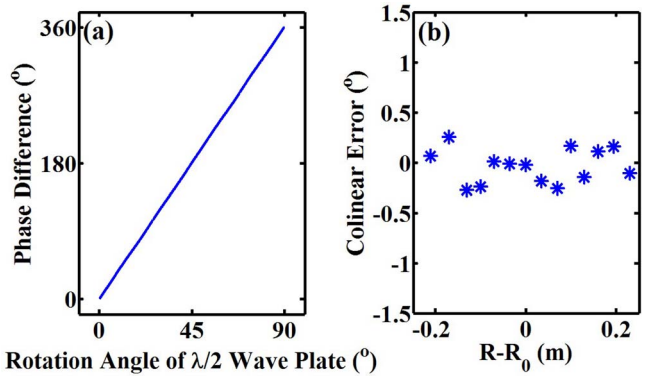

FIG. 2. Calibration results of (a) polarization of probe beams and (b) colinear error for 14 chords in high density J-TEXT experiment.

plasma experiment. By setting the polarization of the probe beams to linear (by simply placing a linear polarizer in front of the probe beam) and measuring the phase difference during plasma operation, any observed phase difference results from misalignment. Using this method, the collinearity of J-TEXT POLARIS is checked, as shown in Figure 2(b). Fourteen chords are used in the test to obtain the error profile where the central line-averaged density for this case is 3.5×10^{19} m^{-3}, which is a high density discharge for J-TEXT. As shown in the figure, the collinearity error is less than 0.2° for almost all chords, smaller than the Faraday angle in this case.

D. Long-term stability

IF and laser power play important roles in three-wave measurement. To correctly extract the phase information carried by each intermediate frequency, the IFs are required to maintain a specified separation (in frequency) and stability. The output laser power, which is directly associated with the SNR of the measurement, must also be fixed at the optimal level for high resolution measurement. However, the intermediate frequency and laser power are vulnerable to long term drifts. Normally the intermediate frequency and the laser power are drift, on average, ∼5 kHz/min and 2%/10 min, respectively. This occurs mainly due to a slow change of the FIR cavity length. To maintain stable performance required for long-term operation, real-time intermediate frequency, and laser power feedback control is necessary.

On J-TEXT POLARIS, a real-time feedback control system has been developed to simultaneously stabilize the intermediate frequencies and laser power by controlling the cavity lengths of each FIR laser. In the feedback control loop, the monitor signals of each IF is directly provided by reference mixer and the laser power is provided by built-in pyro detectors for each FIR laser. No additional optical components are introduced; therefore no modification of the optical layout is required. These monitor signals are digitized and processed by a digital signal processor (DSP) module and then corresponding control signals are sent to each actuator: the PZT controller for each FIR laser. For the IFs, they are directly feedback controlled to the pre-set values, normally 1 MHz, 1.5 MHz, and 2.5 MHz. For laser power, the output power of one master FIR cavity is maintained at the maximum value while the other two lasers are then automatically kept at the optimal power level through the intermediate frequency control. Using this feedback control system, the drifts of IFs are controlled within 10 kHz while the laser power is stabilized at the optimized level. There is no time limit for this feedback control system and it is now routinely used on J-TEXT POLARIS to sustain the performance of the system during daily operation.

III. EXPERIMENTAL RESULTS

A. Overview

Typical multi-chord polarimetry-interferometry data from the J-TEXT POLARIS are presented in Fig. 3. There are 14 chords with impact parameter x = 0.24 m, 0.21 m, 0.18 m, 0.15 m, 0.12 m, 0.09 m, 0.05 m, 0.01 m, 0.03 m, −0.07 m, −0.11 m, −0.15 m, −0.18 m, and −0.206 m (0 denotes the position of major radius and positive value corresponds to low field side), covering ∼90% of the plasma cross section. The phase resolution for each chord is ∼0.05° for Faraday angle and ∼1° for line-integrated density averagely for bandwidth of 50 kHz.

From the multi-chord measurement, spatial profiles of Faraday angle, and line-integrated density are obtained, as shown in Figs. 3(d) and 3(e). As the Faraday angle is associated with the projected magnetic field along the beam path, the sign of Faraday angle for high field and low field sides is opposite, where the direction of poloidal magnetic field is reversed. When the poloidal magnetic field is perpendicular to the probe beam path, Faraday angle equals zero, which corresponds to the zero point of the Faraday profile. This point can be approximately considered as the position of magnetic axis and the slope of Faraday angle across this point is associated with central current density.[15] With the spatial profiles of Faraday angle and line-integrated density from POLARIS, equilibrium reconstruction can be performed and profiles of the current density profile, safety factor and electron density can be obtained.[16–18] In addition to equilibrium information, benefitting from the high resolution, magnetic and density perturbations associated with MHD activity are also observed. As can be seen from Figs. 3(b) and 3(c), both Faraday angle and line-integrated density data exhibit high-frequency response from 0.07 s to 0.13 s, which are associated with tearing mode activity. After the tearing activity ceases (0.13 s), sawtooth activity gradually appears at ∼0.2 s. This activity can be seen on both Faraday angle and line-integrated density from 0.2 s to 0.35 s. With multi-chord measurement, the perturbation spatial distribution of the perturbation is directly obtained. In the following, several examples regarding equilibrium dynamics and perturbations measured using the J-TEXT POLARIS are presented.

B. Sawtooth and tearing mode

Sawtooth perturbations observed by J-TEXT POLARIS are presented in Fig. 4. Temporal traces of Faraday angle and line-integrated density perturbations for 14 chords are shown in Figs. 4(a) and 4(b), while the temporal evolutions of their spatial profiles are plotted in Figs. 4(c) and 4(d). Both

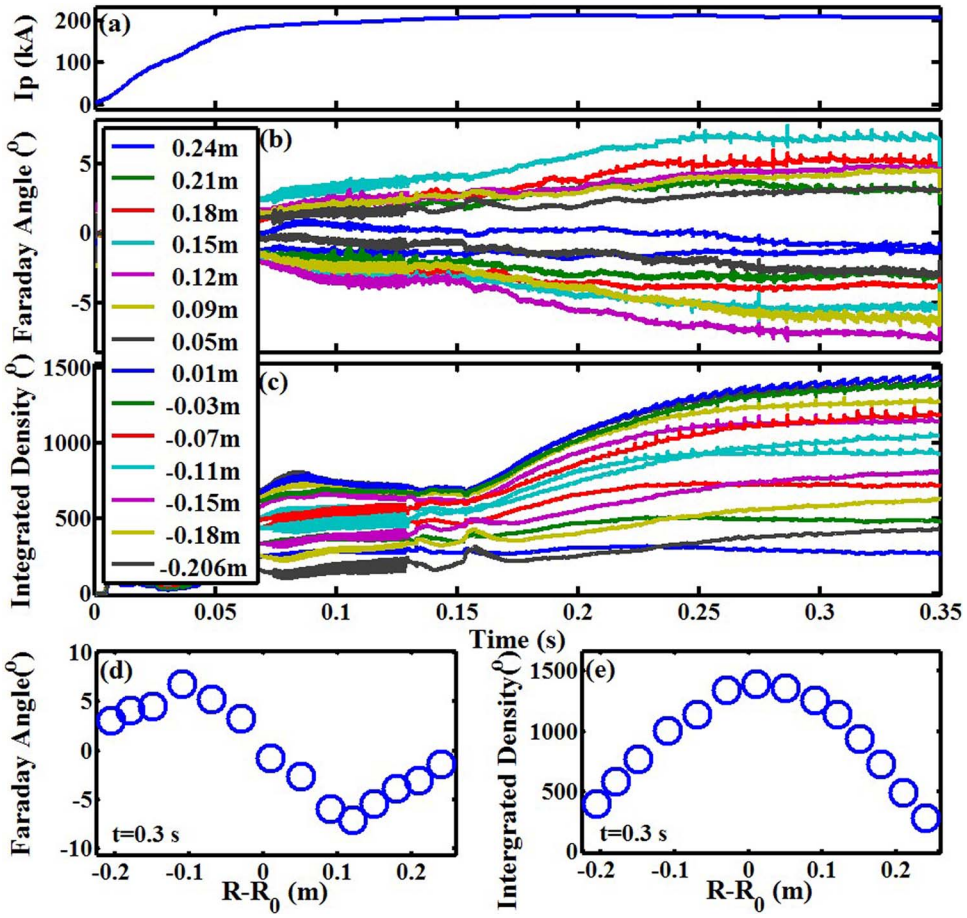

FIG. 3. Typical experimental results from J-TEXT POLARIS. (a) Plasma current, (b) 14 chords Faraday angle, and (c) 14 chords line-integrated density. Spatial profile of (d) Faraday angle and (e) line-integrated density in t = 0.3 s.

sawtooth and inverse sawtooth behaviors are directly observed on Faraday angle and line-integrated density. The maximum perturbation for Faraday angle and integrated density are ∼0.3° and ∼20°, respectively. For density sawtooth, m = 1 MHD pre-cursor oscillations before sawtooth crash can be clearly seen on central chords, with a maximum value ∼10°, while for Faraday sawtooth no clear oscillation are found. From the contour plots shown in Figs. 4(c) and 4(d), the spatial distribution of sawtooth pattern is clearly different for Faraday-effect and density perturbations. For density sawtooth, central chords exhibit a sawtooth pattern, while chords near edge at low field side and high field side show inverse sawtooth behavior. The electron core density peaks during the linear ramp phase and particles are redistributed to the mixing radius at the sawtooth crash. After the crash, the redistributed particles diffuse to the boundary Position of rational surface q = 1 can be identified from these data. In contrast, the Faraday sawtooth is completely different from density sawtooth, manifesting the role of magnetic perturbation in this process. It is found that within the region of q = 1 surface determined from density sawtooth, both sawtooth, and inversed sawtooth exist for Faraday perturbation. This sawtooth-inversed sawtooth pattern in the core region corresponds to a change of the slope of Faraday angle profile across the magnetic axis, which indicates a change of central current density (flattening at the crash) during the sawtooth cycle.

From equilibrium reconstruction, the temporal evolution of equilibrium current density profile and electron density profile during single sawtooth circle are obtained, as presented in Figure 5. To clearly observe the sawtooth-induced change, mean values of the reconstructed profiles are removed. As can be seen, the behavior of current density profile is analogous to the electron density profile. Both of these profiles peak during the sawtooth linear ramp phase and flatten after the sawtooth crash. For the case shown, the amplitude of change at the center is ∼0.15 MA/m^2 for current density and ∼0.4 × 10^{19} m^{-3} for electron density, ∼6% and ∼10% changes compared to the mean. Both profiles crash simultaneously and the duration of crash is within 0.05 sawtooth period, normally ∼100 μs for J-TEXT case.

Similarly, magnetic and density perturbations during intrinsic tearing mode (m = 2, n = 1) activity are also observed, as shown in Fig. 6. Raw Faraday and density perturbations are plotted in Figs. 6(a) and 6(b), while the temporal evolutions of their spatial profiles are plotted in Figs. 6(c) and 6(d). The maximum amplitude of perturbation is ∼0.3° for Faraday angle and ∼40° for line-integrated density. From the contour plot it is clearly seen there are 4 phase reversal points for density perturbation. The outermost reversal points, ∼−0.17 m at the high field side and ∼0.16 m at low field side, provide approximate markers for the q = 2 rational surface. The phase reversal of density perturbation across the rational surface

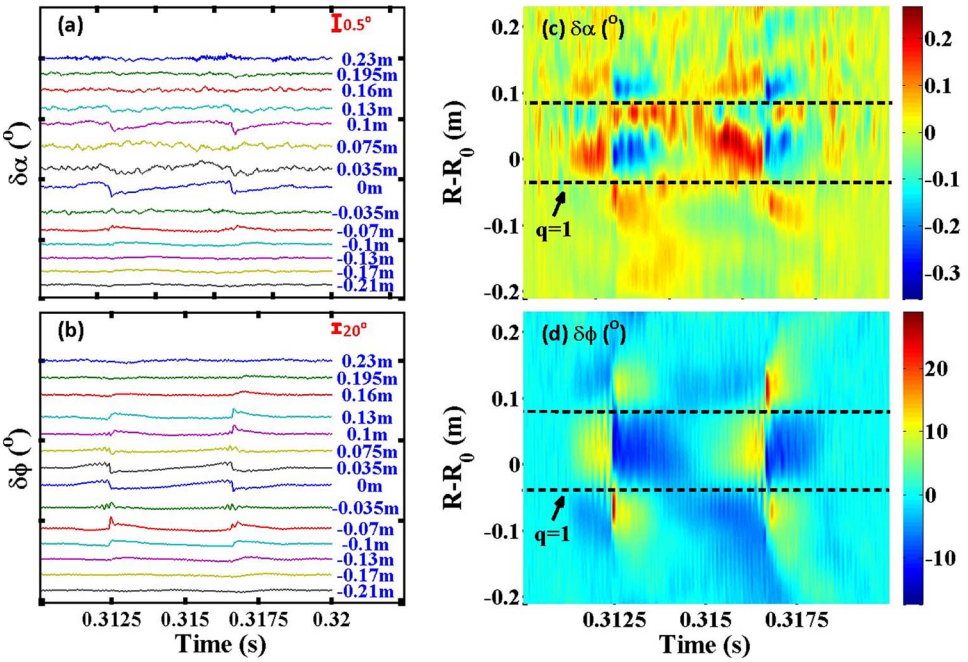

FIG. 4. Typical sawtooth perturbations observed by J-TEXT POLARIS. (a) Faraday perturbation, (b) line-integrated density perturbation, (c) contour plot of temporal evolution of Faraday perturbation profile, and (d) line-integrated density perturbation profile.

indicates flattening of the density across the magnetic island. The other two reversal points in core region are likely introduced by line-integration effects. On the other hand, the Faraday perturbation exhibits a markedly different pattern. The difference between the polarimetry and density perturbations is related to the magnetic information embedded in the Faraday-effect data. Additionally, both perturbations show highly spatial asymmetry between high field side and low field side, which indicates the perturbation structure is largely different, probably caused by toroidal effect.

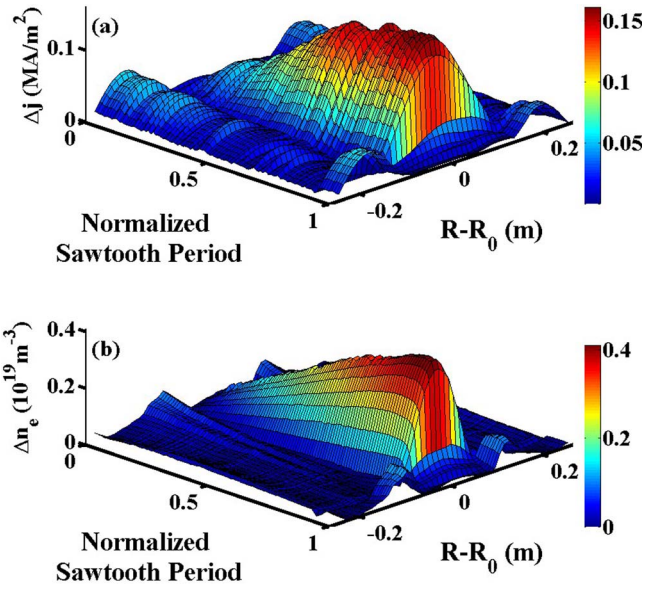

FIG. 5. Evolution of current density profile and electron density profile during single sawtooth cycle. (a) Current density profile and (b) electron density profile.

C. Resonant magnetic perturbation penetration

Externally applied RMP is now considered a powerful tool for plasma control and it has been widely studied in recent years.[19,20] Although RMP is applied for instability control, the mechanism of plasma response to the RMP is still not fully understood, primarily due to lack of internal perturbation measurement. On J-TEXT tokamak, two sets of coils have also been developed to study RMP relevant physics.[21] With POLARIS diagnostic, detailed information for both plasma equilibrium response and magnetic perturbation during the RMP can be obtained.

In Fig. 7, a RMP penetration event on J-TEXT is presented. The plasma current (solid) and RMP current (dashed) are plotted in Figure 7(a), and line-integrated density, Soft-X ray signal, locked-mode signal measured by external magnetic coils and Mirnov signal are plotted in Figs. 7(b)–7(e), in sequence. As can be seen, when the RMP current exceeds a critical value (~6 kA), penetration occurs, denoted by large confinement loss (particles and heat) shown by Figures 7(b) and 7(c). In this process the locked mode signal increases, indicating a locked magnetic island was excited. Because the island was locked, nothing is observed on the Mirnov signal.

Data from POLARIS during this RMP penetration event are shown in Figure 8. The multi-chord line-integrated density and Faraday angle data are presented in Figs. 8(a) and 8(b), respectively; and corresponding results of equilibrium reconstruction, i.e., central safety factor, central current density, and central electron density are plotted in Figs. 8(c)–8(e). According to RMP current, the penetration event can be divided into three phases. In phase 1, when the RMP current was just applied and slowly ramped up, integrated density for most chords slightly decreased by 3%–5%, representing the process of density pump-out. Correspondingly, the change of Faraday angle in phase 1 is very small. In phase 2, when the

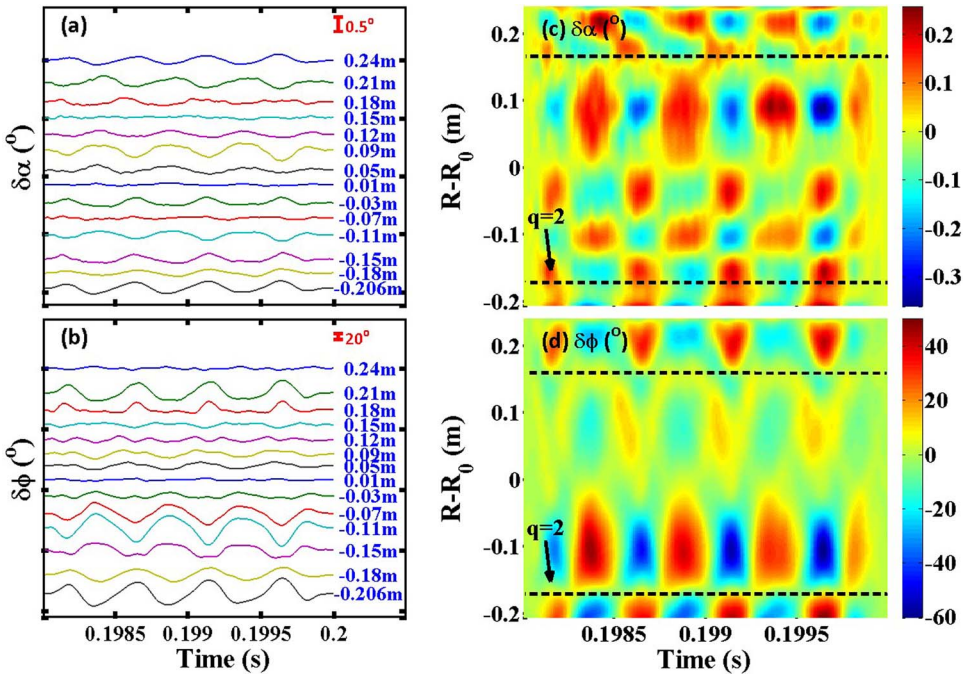

FIG. 6. Typical tearing oscillations observed by J-TEXT POLARIS. (a) Faraday perturbation, (b) line-integrated density perturbation, (c) contour plot of temporal evolution of Faraday perturbation profile, and (d) line-integrated density perturbation profile.

RMP current reached the threshold, penetration begins. Both equilibrium response and perturbation response can be seen on POLARIS data. For integrated density, the density on central chords largely decreases, indicating a large drop of core electron density. The Boundary chords at low field side and high field side Show an asymmetric response, which is likely associated with the excitation of a locked island. For the Faraday angle there is a similar behavior, however, it is difficult to directly determine the magnetic response from the raw data. In phase 3, when RMP current is reduced, the electron density keeps dropping and the confinement is irreversibly degraded. The difference of Faraday angle and integrated density

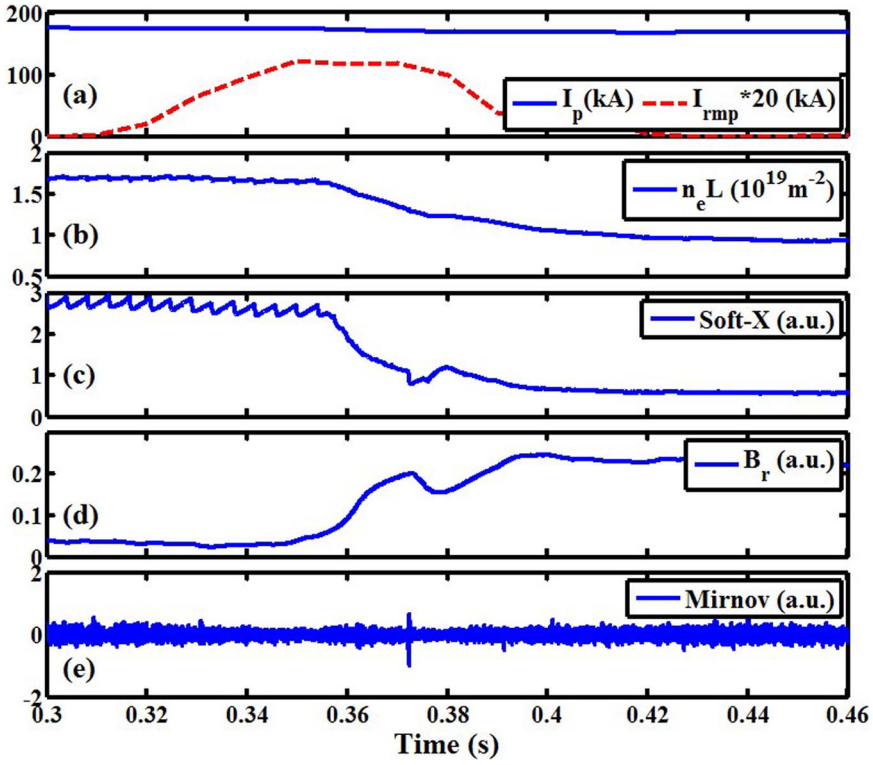

FIG. 7. RMP penetration event on J-TEXT. (a) Plasma current (solid) and RMP current (dashed), (b) line-integrated density, (c) line-integrated Soft-X ray signal, (d) locked-mode signal from external magnetic coils, and (e) Mirnov signal.

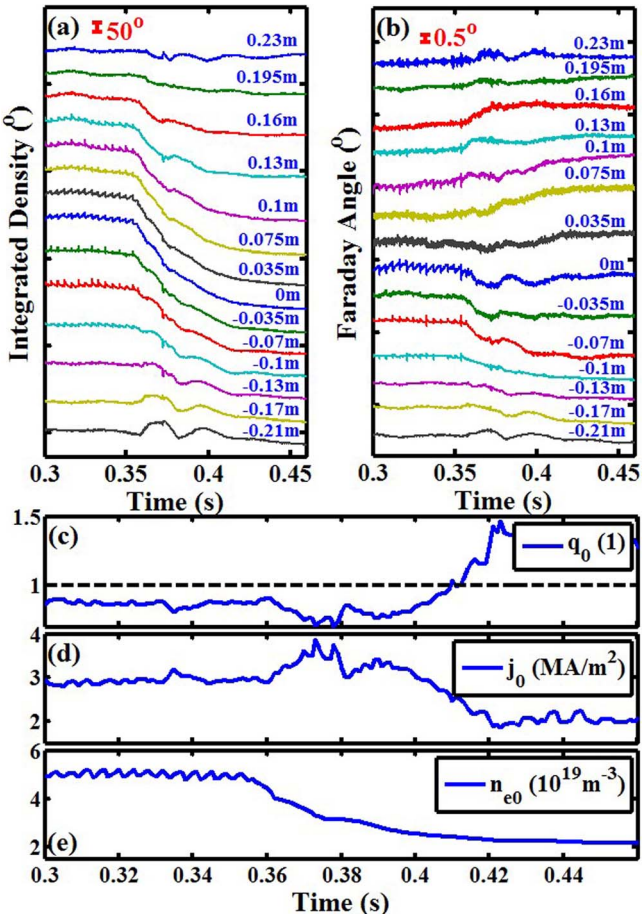

FIG. 8. Multi-chord Faraday angle, line-integrated density, and result of equilibrium reconstruction during RMP penetration event. (a) Line-integrated density, (b) Faraday angle, (c) central safety factor, (d) central current density, and (e) central electron density.

before and after the penetration event indicates there are significant changes in the plasma equilibrium, which can be directly seen from results of equilibrium reconstruction. As shown in Figs. 8(c)–8(e), the central current density decreased from 3 MA/m^2 to ~2 MA/m^2 and the electron density dropped from 5×10^{19} m^{-3} to 2×10^{19} m^{-3}, correspondingly the central safety factor increased from ~0.85 to 1.4. The decrease of current density is delayed with respect to the electron density, which may indicate that the electron density (particles) and current density (magnetic) play different roles during the equilibrium response to the RMP.

IV. SUMMARY

A three-wave laser-based high-resolution polarimeter-interferometer system (POLARIS) for simultaneous Faraday and line-integrated density measurement has been developed on the J-TEXT tokamak. The system temporal resolution is ~1 μs; phase resolution for Faraday angle is $<0.05^\circ$ and interferometer phase is $<1^\circ$ for 50 kHz bandwidth. Measurement with 14 chords, ~35 mm chord spacing, has been achieved, covering 90% of the plasma cross section. The system can be readily upgraded to 36 chords with 15 mm chord spacing in the future. Fast plasma equilibrium dynamics along with magnetic and density perturbations are resolved by the high resolution system. Non-axisymmetric effects, related to intrinsic tearing modes and penetration of 3D resonant magnetic perturbation are directly measured. Resolving the local structure of magnetic and electron density perturbations will be the focus of future investigations.

ACKNOWLEDGMENTS

The authors would like to thank all the engineers and technicians on J-TEXT for their support and assistance to the project. This work is supported by the ITER Project Funds of People's Republic of China: Contract Nos. 2013GB106001 and 2009GB107003, and partly supported by the JSPS-NRF-NSFC A3 Foresight Program in the field of Plasma Physics (NSFC No. 11261140328).

[1]A. J. H. Donné *et al.*, Nucl. Fusion **47**, S337–S384 (2007).
[2]F. D. Marco and S. E. Segre, Plasma Phys. **14**, 245 (1972).
[3]G. Dodel and W. Kunz, Infrared Phys. **18**, 773 (1978).
[4]D. L. Brower *et al.*, Rev. Sci. Instrum. **74**, 1534 (2003).
[5]W. F. Bergerson, P. Xu, J. H. Irby, D. L. Brower, W. X. Ding, and E. S. Marmar, Rev. Sci. Instrum. **83**, 10E316 (2012).
[6]G. Zhuang *et al.*, Nucl. Fusion **53**, 104014 (2013).
[7]J. Chen, G. Zhuang, Z. J. Wang, L. Gao, Q. Li, W. Chen, D. L. Brower, and W. X. Ding, Rev. Sci. Instrum. **83**, 10E306 (2012).
[8]G. Zhuang, J. Chen, Q. Li, L. Gao, Z. J. Wang, Y. Liu, and W. Chen, J. Instrum. **8**, C10019 (2013).
[9]Y. Jiang, D. L. Brower, L. Zeng, and J. Howard, Rev. Sci. Instrum. **68**, 902 (1997).
[10]W. X. Ding, D. L. Brower, W. F. Bergerson, and L. Lin, Rev. Sci. Instrum. **81**, 10D508 (2010).
[11]V. V. Mirnov, W. X. Ding, D. L. Brower, M. A. Van Zeeland, and T. N. Carlstrom, Phys. Plasmas **14**, 102105 (2007).
[12]R. Imazawa, Y. Kawano, and Y. Kusama, Plasma Phys. Controlled Fusion **54**, 055005 (2012).
[13]D. L. Brower, Y. Jiang, W. X. Ding, S. D. Terry, N. E. Lanier, J. K. Anderson, C. B. Forest, and D. Holly, Rev. Sci. Instrum. **72**, 1077 (2001).
[14]L. Lin, W. X. Ding, and D. L. Brower, Rev. Sci. Instrum. **83**, 10E320 (2012).
[15]D. L. Brower, W. X. Ding, S. D. Terry *et al.*, Phys. Rev. Lett. **88**, 185005 (2002).
[16]H. Soltwisch, Rev. Sci. Instrum. **57**(8), 1939 (1986).
[17]B. W. Rice and E. B. Hooper, Nucl. Fusion **34**, 1 (1994).
[18]L. Zeng, D. L. Brower, and Y. Jiang, Plasma Phys. Controlled Fusion **39**, 591–608 (1997).
[19]T. C. Hender *et al.*, Nucl. Fusion **32**, 1091 (1992).
[20]R. Fitzpatrick, Nucl. Fusion **33**, 1049 (1993).
[21]B. Rao *et al.*, Fusion Eng. Des. **89**, 378–384 (2014).